IEEE Access
Multidisciplinary | Rapid Review | Open Access Journal

Received October 12, 2021, accepted November 2, 2021, date of publication November 8, 2021, date of current version November 15, 2021.

Digital Object Identifier 10.1109/ACCESS.2021.3126322

Photonics-Assisted Multi-Band Dual Linear/Nonlinear Chirp Waveform Generation Based on Optical Phase Modulation

HONGSHI ZHAO AND JIANXIN MA, (Member, IEEE)
State Key Laboratory of Information Photonics and Optical Communications, Beijing 100876, China
Beijing Key Laboratory of Space-Ground Interconnection and Convergence, Beijing 100876, China
School of Electronic Engineering, Beijing University of Posts and Telecommunications, Beijing 100876, China

Corresponding author: Jianxin Ma (majianxinxy@163.com)

This work was supported in part by the National Natural Science Foundation of China under Grant 61690195, and in part by the Fund of State Key Laboratory of IPOC under Grant IPOC2020ZT06.

ABSTRACT A novel photonic scheme for generating multi-band dual-chirp waveforms with linear or nonlinear chirp rates is proposed via two cascaded polarization modulators (PolMs) paralleled with a phase modulator (PM). The cascaded PolMs produce a flat optical frequency comb (OFC) as a multi-frequency reference light, while the PM is driven by the power-function-type baseband signals to obtain the lightwave with different order phase chirp. The phase-chirped lightwave and the multi-frequency reference lightwave are orthogonally coupled by a polarization beam combiner (PBC) and then recombined via a polarization beam splitter (PBS) to make them in-phase in one output port of the PBS and anti-phase in the other. The two recombined lightwaves are detected by a balanced photodetector (BPD), and the different order dual-chirp signals, covering six bands, can be generated in their differential photocurrent without interference components. Compared with the single-chirp signal of the knife-edge-type ambiguity function, the dual-chirp signal with the peak-saliency-type ambiguity function significantly suppresses sidelobes and shows better range-Doppler resolution performance. With the 1GHz-bandwidth and 102.4ns-duration quadratic baseband driving signal, six-band linear dual-chirp signal, centered at 10, 30, 50, 70, 90 and 110GHz, are generated by simulation, and each linear dual-chirp signal has a bandwidth of 4.1GHz, the pulse compression ratio of 465.45 and the peak-to-sidelobe ratio (PSLR) of 12.8dB. As baseband driving signal has higher (3rd) order power, the six-band nonlinear dual-chirp signals with the same central frequencies can also be generated but with increased bandwidth (6.3GHz) and improved PSLR (15.51dB). Their autocorrelation functions show that compared with the linear chirp signal, the nonlinear chirp signal has better sidelobe suppression capability, which is improve as the degree of nonlinearity increase.

INDEX TERMS Microwave photonics, multi-band radar system, dual-chirp waveform, nonlinear chirp waveform.

I. INTRODUCTION

The radar working in different radio spectral regions performs different functions depending on the carrier frequencies utilized. Multi-band radar is the development trend of the next generation performance enhanced radar system for simultaneously implementing different functions, such as detection, tracking, and imaging [1]. Moreover, these functions can be mutually beneficial to improve the radar system performance [2], [3]. Therefore, frequency flexibility, diversity and configurability will be largely desired. Remote tracking and missile guidance radars operating in X- to W-bands (8-110GHz), which require the ability to track the trajectory of multiple targets simultaneously, have high resolution to accurately control the missile attack targets. X-band (8-12GHz) radars are often used to generate narrower beams

The associate editor coordinating the review of this manuscript and approving it for publication was Chengpeng Hao.

with improved spatial resolution for highly resolved target imaging. Ku-band (12-18GHz) radars are mainly used for firefighting aircraft and satellite communication. Although Ka-band (27-40GHz) radars are limited in range due to atmospheric attenuation, they have the superior angle and spatial discrimination, so are often used as surface movement radar (SMR) at airports [4]. Unfortunately, due to the inherent narrow band of conventional radio frequency (RF) electronics, multi-band radar can only be implemented by using several independent single-band equipment. The introduction of photonics in radar systems not only assures benefits in terms of large instantaneous bandwidth, low phase noise, low loss, easy tunability, and immunity to electromagnetic interferences (EMI) and eavesdropping [5]–[9], but also overcomes the limitations of conventional electronic devices and provides a promising solution for the future advanced radar system.

Chirp waveforms are widely used in photonic-assisted radar systems to achieve high range resolution. The single-chirp waveform has a knife-edge-type ambiguity function with large range-Doppler coupling, and the Doppler resolution is substantial loss, which makes it impossible to accurately distinguish closely moving targets. While the dual-chirp waveform, consisting of two complementarily single-chirp waveforms within the same time duration, has better range-Doppler resolution due to its smaller range-Doppler coupling, and is being studied in radar systems. An integrated dual-polarization quadrature phase shift keying (DP-QPSK) modulator is used to photonically generate frequency-quadrupling dual-band chirp signals [10], or dual-band dual-chirp microwave waveforms with multiplying central frequency and bandwidth [11]. Although frequency-multiplexed dual-band chirp waveforms can be generated by using polarization selection, four sub-MZMs and six bias voltages must be adjusted simultaneously to generate the required sidebands, which undoubtedly increases the operational complexity. In addition, the dual-band waveforms generated by two subsystems are driven by multiple local baseband waveforms, which also increases the system cost. To simplify the structure, a photonic approach to generate multi-frequency dual-chirp waveform is proposed by using a dual-polarization Mach-Zehnder modulator (DPol-MZM) with a balanced photodiode [12], while multiple local baseband waveforms are still needed. In addition, the baseband waveform is required to drive the sub-MZM to intensity modulate the input lightwave, and the undesirable chirp interference signals will inevitably associated after photoelectric conversion.

Linear chirp waveforms with large time bandwidth product (TBWP) have higher range resolution due to their better pulse compression capability, and have been applied to radar systems widely. But the compressed pulse of the linear chirp signal after matched filtering has a low peak-to-sidelobe ratio (PSLR), which may mask the returning echoes of targets adjacent to the main target. So nonlinear chirp waveforms are expected to solve this problem. The nonlinear chirp signal has a faster frequency sweep rate at the pulse edges and a slower frequency sweep rate at the pulse center, which means better PSLR after pulse compression, good interference mitigation, improved signal-to-noise ratio (SNR) and enhanced useful dynamic range of radar systems [13]–[15]. Photonic generation of nonlinear chirp waveforms have rarely been reported. In [16], the nonlinear chirp waveform is generated based on current modulation of a distributed feedback laser diode (DFB-LD) in a self-heterodyne scheme, while both bandwidth and tuning ability of the generated nonlinear chirp signal are limited. In [17], the nonlinear frequency modulated (NLFM) microwave waveform is generated based on controlled period-one (P1) dynamics of an optically injected semiconductor laser (OISL). The microwave frequency output is closely related to the optical injection strength controlled by the modulation voltage input. Although both nonlinear single-chirp and dual-chirp microwave waveforms are generated, the scheme has poor frequency adjustability, and it is difficult to extend to multiple frequency bands.

In this paper, a novel photonic scheme for generating multi-band dual linear/nonlinear chirp waveform is proposed and analyzed. The cascaded polarization modulators (PolMs) driven by radio frequency (RF) produce a 12-lines optical frequency comb (OFC) as a multi-frequency reference light. The phase modulator (PM) is driven by the power-function-type signal to modulate the phase of the lightwave for obtaining the different order phase-chirped signals. The phase-changing signal light is then orthogonally coupled with the multi-frequency reference light. By adjusting the polarization angles of the polarization beam splitter (PBS) to 45° and 135°, the polarization multiplexed lightwave are recombined with equal amplitude and opposite phase and detected by balanced PD to eliminate the high frequency components that would be produced in the heterodyne beating. The proposed waveform generator is implemented by simulation and six-bands bandwidth-multiplexed linear or nonlinear dual-chirp waveforms, covering X- to W-band, are generated. Since the lightwave is only phase modulated in the system, the waveforms obtained has pure spectra, without undesired chirp and high frequency interferences. Moreover, the generated dual chirp waveforms have adjustable frequency and bandwidth and good pulse compression capability. In addition, according to the analysis of the auto-correlation function, the nonlinear chirp signal has better PSLR compared with the linear chirp signal. In fact, the PSLR improves as the degree of nonlinearity increases. It is expected that the multi-function radar system with our proposed multi-band dual-chirp waveforms generation scheme has better performance.

II. PRINCIPLE

The schematic diagram of the proposed multi-band dual-chirp waveform generator based on optical phase modulation is shown in Fig. 1. The linearly polarized lightwave emitted from a laser diode (LD) is split into two beams with equal power by an optical coupler (OC). The upper beam is coupled

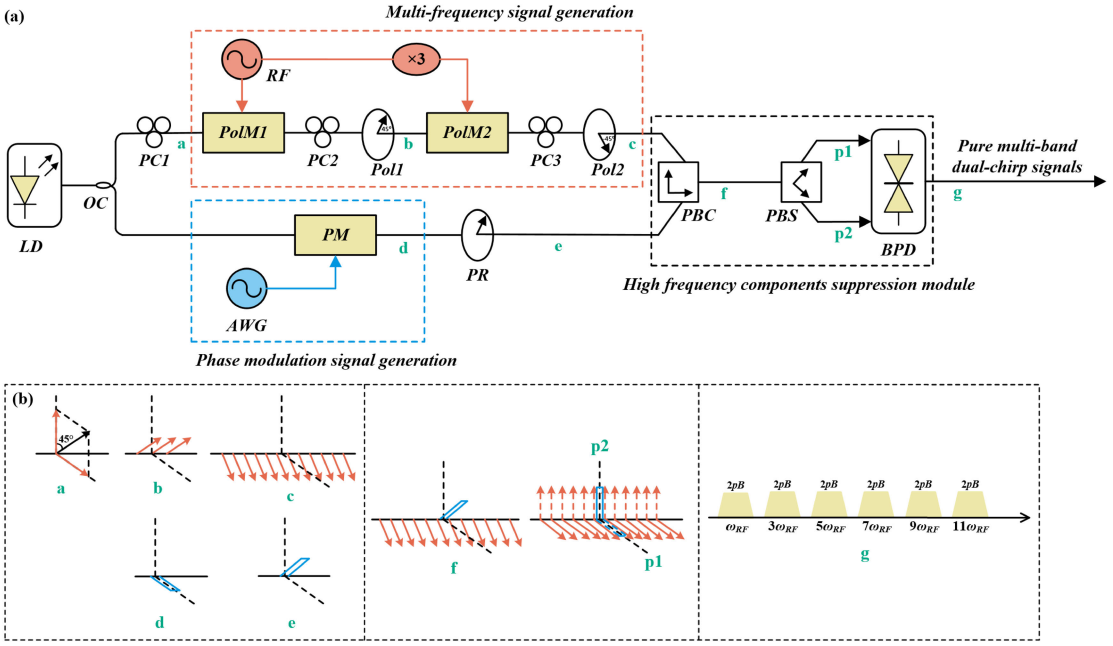

FIGURE 1. (a) Schematic diagram of the proposed multi-band dual-chirp waveform generator. LD: laser diode; OC: optical coupler; PC: polarization controller; RF: radio frequency; PolM: polarization modulator; Pol: polarizer; AWG: arbitrary waveform generator; PM: phase modulator; PR: polarization rotator; PBC: polarization beam combiner; PBS: polarization beam splitter; BPD: balanced photodetector, (b) evolution of the polarization directions.

into the cascaded PolMs module for RF modulation to obtain a multi-tone reference light, while the lower beam is coupled into the PM driven by the power-function-type baseband signal from an arbitrary waveform generator (AWG) to introduce the phase chirp.

The upper beam is oriented at an angle of 45° to one principal axis of PolM1 by polarization controller (PC). The PolM1 is driven by a RF signal with an angular frequency of ω_{RF}. Here the PolM is equivalent to two phase modulators along the two principal axes, and so a pair of optical signals in two polarization directions perpendicular to each other are modulated by the RF signal with complementary modulation indices. The output of PolM1 can be expressed in Jones matrix as

$$\begin{pmatrix} E_{PolM1x}(t) \\ E_{PolM1y}(t) \end{pmatrix} = \frac{\sqrt{2}}{2} E_{in}(t) \begin{pmatrix} e^{j\beta_1 \cos \omega_{RF} t} \\ e^{-j\beta_1 \cos \omega_{RF} t} \end{pmatrix} \tag{1}$$

where $E_{\text{in}}(t) = E_0 \exp(j\omega_0 t)$ denotes the output of LD with the amplitude of E_0 and angular frequency of ω_0, $\beta_1 = \pi V_{RF1}/V_\pi$ is the modulation index of PolM1 with the half-wave voltage of V_π, and V_{RF1} is the amplitude of the RF signal. The two orthogonal lightwaves in Eq. (1) are recombined into a linearly polarized lightwave by a polarizer (Pol) that is oriented at 45° to one principal axis of the PolM1 after the polarization direction is adjusted by the PC, so it can be expressed as

$$\begin{aligned} E_{Pol1}(t) &= E_{PolM1x}(t)\cos(45°) + E_{PolM1y}(t)\sin(45°) \\ &= \frac{1}{2} E_{in}(t) \left[e^{j\beta_1 \cos \omega_{RF} t} + e^{-j\beta_1 \cos \omega_{RF} t} \right] \\ &= \frac{1}{2} E_{in}(t) \left[\sum_{n=-\infty}^{+\infty} j^n J_n(\beta_1) e^{jn\omega_{RF} t} \right. \\ &\qquad \left. + \sum_{n=-\infty}^{+\infty} (-1)^n j^n J_n(\beta_1) e^{jn\omega_{RF} t} \right] \\ &= \frac{1}{2} E_{in}(t) \sum_{n=-\infty}^{+\infty} \left[1 + (-1)^n \right] j^n J_n(\beta_1) e^{jn\omega_{RF} t} \end{aligned} \tag{2}$$

where $J_n(\cdot)$ is the n^{th}-order Bessel function of the first kind. With the Jacob-Anger expansions of exponential-functions and summarization, only the even-order sidebands are output while the odd-order sidebands are suppressed. Then, similarly, the linearized multi-tone lightwave is injected into the PolM2 for modulation by the RF signal with an angular frequency of $3\omega_{RF}$, and the output lightwave becomes

$$\begin{pmatrix} E_{PolM2x}(t) \\ E_{PolM2y}(t) \end{pmatrix} = \frac{\sqrt{2}}{2} E_{pol1}(t) \begin{pmatrix} e^{j\beta_2 \cos 3\omega_{RF} t} \\ e^{-j\beta_2 \cos 3\omega_{RF} t} \end{pmatrix} \tag{3}$$

where $\beta_2 = \pi V_{RF2}/V_\pi$ is the modulation index of PolM2. The Pol2 is oriented at −45° to the principal axes of the PolM2 to suppress the even-order sidebands, so only the odd-order sidebands are obtained and can be expressed as

$$\begin{aligned} E_{pol2}(t) &= E_{PolM2x}(t)\cos(-45°) + E_{PolM2y}(t)\sin(-45°) \\ &= \frac{1}{2} E_{Pol1}(t) \left[e^{j\beta_2 \cos 3\omega_{RF}} - e^{-j\beta_2 \cos 3\omega_{RF} t} \right] \\ &= \frac{1}{4} E_{in}(t) \left\{ \sum_{n=-\infty}^{+\infty} \left[1 + (-1)^n \right] j^n J_n(\beta_1) e^{jn\omega_{RF} t} \right\} \end{aligned}$$

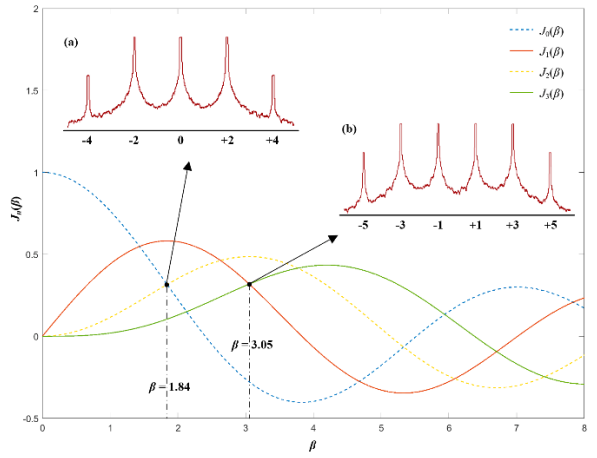

FIGURE 2. Relationship between β and $J_n(\beta)$.

$$\cdot \left\{ \sum_{m=-\infty}^{+\infty} \left[1-(-1)^m\right] j^m J_m(\beta_2)\, e^{j3m\omega_{RF}t} \right\} \quad (4)$$

According to the Bessel functions of the first kind $J_n(\beta)$, shown in Fig. 2, if $\beta_1 = 1.84$, there is $J_0(\beta_1) = J_2(\beta_1)$, which means that the optical carrier and $\pm$2nd-order sidebands have equal amplitudes; Moreover, if $\beta_2 = 3.05$, $J_1(\beta_2) = J_3(\beta_2)$, so the amplitudes of $\pm$1st-order sidebands and $\pm$3rd-order sidebands are equal. Since the other higher sidebands are smaller, Eq. (4) can be simplified as

$$\begin{aligned} E_{pol2}(t) &\approx \frac{1}{4}E_{in}(t)\left[2J_0(1.84) - 2J_2(1.84)e^{2j\omega_{RF}t} \right. \\ &\qquad \left. -2J_2(1.84)e^{-2j\omega_{RF}t}\right] \\ &\quad \cdot \begin{bmatrix} 2jJ_1(3.05)e^{3j\omega_{RF}t} + 2jJ_1(3.05)e^{-3j\omega_{RF}t} \\ -2jJ_3(3.05)e^{9j\omega_{RF}t} - 2jJ_3(3.05)e^{-9j\omega_{RF}} \end{bmatrix} \\ &= E_{in}(t)J_0(1.84)J_1(3.05)j \\ &\quad \begin{bmatrix} e^{j\omega_{RF}t} - e^{-j\omega_{RF}t} + e^{3j\omega_{RF}t} + e^{-3j\omega_{RF}t} \\ -e^{5j\omega_{RF}t} - e^{-5j\omega_{RF}t} + e^{7j\omega_{RF}t} + e^{-7j\omega_{RF}t} \\ -e^{9j\omega_{RF}t} - e^{-9j\omega_{RF}t} + e^{11j\omega_{RF}t} + e^{-11j\omega_{RF}t} \end{bmatrix} \end{aligned} \quad (5)$$

As can be seen in Eq. (5), the output lightwave includes 12 equal amplitude tones with frequencies at $\pm\omega_{RF}$, $\pm3\omega_{RF}$, $\pm5\omega_{RF}$, $\pm7\omega_{RF}$, $\pm9\omega_{RF}$, and $\pm11\omega_{RF}$, forming a 12-lines OFC.

The lower beam from the LD is phase modulated via a PM by the power-function-type baseband signal $S(t) = kt^p$ from an AWG, and becomes

$$E_{pm}(t) = E_{in}(t)\exp(j\beta_3 kt^p) \quad (6)$$

where β_3 is the modulation index of the PM. After rotated 45° by a polarization rotator (PR), the output lightwave $E_{pm}(t)$ is polarization-orthogonal coupled with the generated OFC from the upper branch via a polarization beam combiner (PBC), so the output of PBC can be expressed as

$$E_{PBC}(t) = \hat{x}E_{pol2} + \hat{y}E_{pm} = \begin{bmatrix} E_{pol2}(t) \\ E_{pm}(t) \end{bmatrix} \quad (7)$$

Then, the OFC and the phase-modulated chirp lightwave on the two polarization state are recombined via a polarization beam splitter (PBS), whose the polarization axes have angles of 45° relative to one lightwave, so there are

$$E_{P1}(t) = E_{pol2}(t)\cos(45°) + E_{pm}(t)\sin(45°) \quad (8)$$

$$E_{P2}(t) = E_{pol2}(t)\cos(135°) + E_{pm}(t)\sin(135°) \quad (9)$$

It can be seen that each of the recombined lightwaves include the OFC and the phase-modulated chirp lightwave, but the two components have different relative phase (180°) in the two beams. Finally, the two recombined lightwaves are simultaneously injected into a balanced photodiode (BPD), consisting two PD with identical parameters and a differential circuit, for photoelectric conversion, and the output differential photocurrent is given as

$$\begin{aligned} I_{BPD}(t) &= \eta\left[E_{p1}(t)E_{p1}^*(t) - E_{p2}(t)E_{p2}^*(t)\right] \\ &\propto 2\eta J_0(1.84)J_1(3.05)E_0^2 \\ &\quad \left[\begin{array}{l} \cos(\omega_{RF}t \pm 2\beta_3 kt^p) + \cos(3\omega_{RF}t \pm 2\beta_3 kt^p) \\ +\cos(5\omega_{RF}t \pm 2\beta_3 kt^p) + \cos(7\omega_{RF}t \pm 2\beta_3 kt^p) \\ +\cos(9\omega_{RF}t \pm 2\beta_3 kt^p) + \cos(11\omega_{RF}t \pm 2\beta_3 kt^p) \end{array}\right] \end{aligned} \quad (10)$$

where η denotes the responsivity of each photodiode in the BPD and $*$ is conjugate operator. It can be seen from Eq. (10) that the output photocurrent consists only of 12 chirp tones, the DC and cross beating components are cancelled out perfectly in the differential circuit because they have identical non-negative amplitudes. Since each two chirp tones with complementary chirp rates and adjacent in the frequency domain form a dual-chirp signal, there are six-bands dual-chirp signals with the center frequencies of ω_{RF}, $3\omega_{RF}$, $5\omega_{RF}$, $7\omega_{RF}$, $9\omega_{RF}$ and $11\omega_{RF}$ in the photocurrent. For each dual-chirp signal, no undesirable chirp components are generated after photoelectric conversion, which will interfere with the useful signals and thus affect the resolution capability of the radar system. This attribute to the use of baseband signal and only modulates the phase of the input lightwave via the PM. No undesirable sidebands appear in the phase-modulated chirp lightwaves, so each RF dual-chirp signal will never suffered from the higher-order linear/nonlinear chirp. Compared with the schemes of introducing frequency chirp by intensity modulation [10]–[12], the proposed scheme can avoid high-order sidebands in the chirp signal generation process, thus minimizing the clutter interference of the required dual-chirp signals.

Since the instantaneous frequency of the RF signal is equal to the differential of its phase, we can generate both linear and nonlinear dual-chirp signals by using different driving baseband signal $S(t)$ applied to the PM. If the power-function-type baseband signal $S(t) = kt^p$ has a quadratic form ($p = 2$, parabolic signal), the linear six-band dual-chirp signals with each bandwidth of $4\beta_3 B$ (bandwidth of the baseband drive signal is B) and chirps rate of $\pm k$ can be obtained. As $p > 2$, the nonlinear dual-chirp signals are obtained. The generated

six-band nonlinear dual-chirp signals have a bandwidth of $2p\beta_3$ times the drive signal bandwidth each, although their central frequencies are the same as that of the linear ones. For both cases, the center frequencies and bandwidth of the six-band dual-chirp signals can be adjusted by tuning the RF frequency ω_{RF}, the chirp rate k and the time duration t, respectively.

In addition, compared with the system based on $LiNbO_3$ Mach-Zehnder intensity modulator to introduce phase chirp on the lightwave suffering from the direct current (DC) bias drifting, both the PolM and PM used in this scheme do not require the DC bias, avoiding the complicated circuit structure for controlling the bias voltage, thus, the generated multi-band dual-chirp signals have high stability and the system configuration is simplified relatively. Meanwhile, the PolM and PM have low insertion loss, which means a higher conversion efficiency.

III. SIMULATION RESULTS AND DISCUSSIONS

To demonstrate the feasibility of the proposed scheme based on the parallel PolM and PM to generate multi-band linear/nonlinear dual-chirp signals, a simulation setup based on Fig. 1 was built.

The LD with a frequency of 193.1THz, a power of 16dBm, and a linewidth of 10MHz is used to emit the linearly polarized lightwave, and its output spectrum is shown in Fig. 3(a). Then, a 1 × 2 optical coupler is used to split the lightwave into two beams with equal power. After the polarization state assigning by a PC, the upper beam is modulated by the RF signals via the cascaded PolMs to generate the 12-lines OFC. The first PolM (PolM1) is driven by a 10GHz RF signal from a local oscillator with the modulation index $\beta_1 = 1.84$, and a polarizer (Pol1) oriented at 45° to the principal axis of PolM1 is used to map the two orthogonally polarized lightwaves to one polarization direction. A 3-lines OFC with the tones at 193.08THz, 193.1THz and 193.12THz is obtained, as shown by the optical spectrum in Fig. 3(b), which agrees with the theoretical analysis. Then, the 3-lines OFC is further modulated via PolM2 by the RF signal with the frequency triple that of PolM1 with the modulation index $\beta_2 = 3.05$. A second polarizer (Pol2), oriented at −45° to the principal axis of PolM2, is used to map the two orthogonally polarized lightwaves to one polarization direction and so a 12-lines OFC with approximately equal amplitude is generated with the frequencies located from 192.99THz to 193.21THz with a frequency spacing of 20GHz, as shown in the optical spectrum in Fig. 3(c). It can be seen that twelve optical tones are at least 14dB higher than the others aside and form a flat OFC. Although some sidelobes appear aside, they are insignificant.

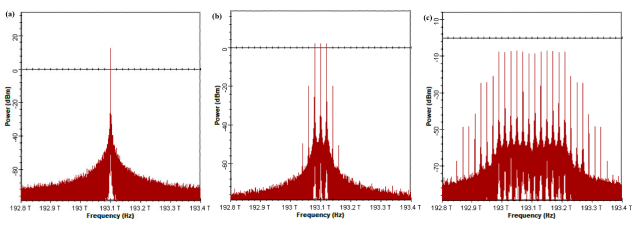

FIGURE 3. Output spectra (a) LD, (b) the 3-lines OFC after Pol1, (c) the 12-lines OFC after Pol2.

The lower beam from the LD is modulated by the different order power-function-type baseband signals from the AWG via a PM with a modulation index $\beta_3 = 1$ to introduce different order phase chirp. Here, 2nd-, 3rd-, 4th-, and 5th-order baseband drive signals, as shown in Fig. 4(a), are applied to the PM, and the corresponding optical spectra output from PM are shown in Fig. 4(b). It can be seen that as the order of the drive signal increases, the bandwidth of the chirp signal increases. Since the time duration T is fixed, the slope of the edge region of the power spectrum envelope does not changes compared to the variation of bandwidth.

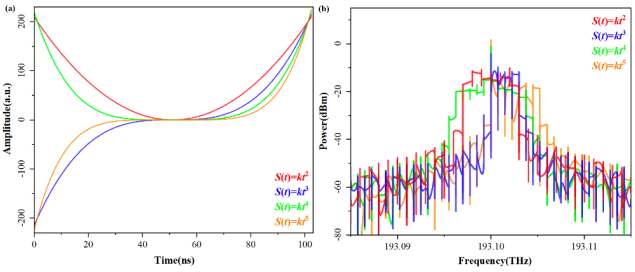

FIGURE 4. (a) PM drive signals, (b) PM output spectra corresponding to different order drive signals.

After the PR rotation to make the OFC and the phase-chirped lightwave from both the cascaded PolMs and the PM polarization-orthogonal, two orthogonally polarized lightwaves are combined orthogonally by a PBC. The spectra of the orthogonal combined lightwaves is shown in Fig.5 with the phase-chirped lightwave at the phase chirp order of 2, 3, 4, and 5.

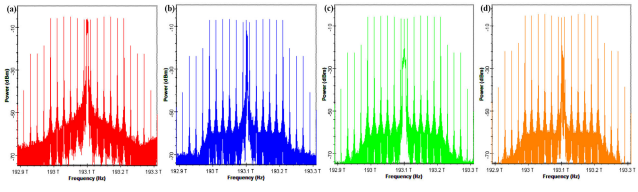

FIGURE 5. PBC output spectra corresponding to different order phase-chirped signals (a) p = 2, (b) p = 3, (c) p = 4, (d) p = 5 (p is the order in the power-function-type baseband drive signal).

Then, a PBS, with the principle axes having a 45° polarization direction rotation relative to the PBC ahead, is used to recombine the orthogonal OFC and phase-chirped lightwave by orthogonal mapping. So two linearly polarized lightwaves output from the PBS containing both orthogonal OFC and phase-chirped lightwave with equal amplitude but opposite relative phase. The two linearly polarized lightwaves are injected into a BPD for photoelectric conversion with the responsivity of 1A/W, dark current of 10nA, and thermal noise of 1 × 10.22W/Hz. The differential photocurrent

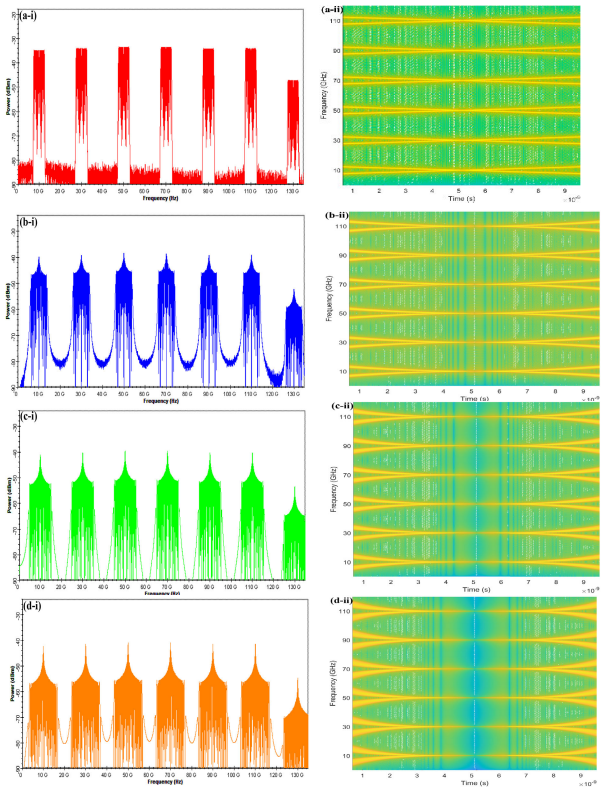

FIGURE 6. (i) spectra and (ii) instantaneous frequency of the multi-band dual-chirp signals with different order phase chirp (a) $p = 2$ (linear chirp), (b) p = 3, (c) $p = 4$, (d) $p = 5$.

includes multi-band dual chirp signals. Fig. 6 gives the generated multi-band dual linear and different order nonlinear chirp spectra, and their instantaneous frequency-time diagrams calculated based on short-time Fourier transform (STFT).

It can be seen from Fig. 6(a-i) to 6(d-i) that when the phase of the lightwave is chirped with the 2-order power function, the generated six-band RF signals with the center frequencies at 10GHz, 30GHz, 50GHz, 70GHz, 90GHz, and 110GHz have linear dual chirp waveforms with an individual bandwidth of 4.1GHz. As the power order of the driving phase-chirped signal increases to 3, 4 and 5, the frequency changes instantaneously and nonlinearly over the time duration, and the bandwidth of dual chirp waveforms increases to 6.3GHz, 8.6GHz, and 12.8GHz, respectively. Since the lower beam only performs phase modulation, no undesirable chirp components are generated after the heterodyne beating, and the self-heterodyne beating components in the photocurrent are completely cancelled out by the balanced photodetection. In our simulation, the generated pure multi-band linear/nonlinear dual-chirp signals cover the X-band (10GHz), Ka-band (30GHz), U-band (50GHz), V-band (70GHz) and W-band (90GHz, 110GHz) of the radar without self-heterodyne beating components and other nonlinearity.

To characterize the generated linear and nonlinear dual-chirp signals by our scheme, a comparative analysis between the linear and nonlinear dual-chirp signals at one band at 10GHz center frequency is conducted. The simulated spectra, waveforms and instantaneous frequencies of the linear and nonlinear dual-chirp signals with the same chirp rate $k = 2\pi \times 10^{16} s^{-2}$, time duration $T = 102.4$ns, but different phase chirp order of p are shown in Fig. 7. From the power spectra in Fig.7(a), it can be seen that the linear dual-chirp signal, with a chirp order of $p = 2$, has a linear frequency chirp and a uniform power spectrum over the 4.1GHz frequency bandwidth, because the probability of being at a particular frequency within the frequency deviation band is the same. While, as the chirp order p increases to 3, 4 and 5, the frequency bandwidth of the corresponding nonlinear dual-chirp signal is extended to 6.3GHz, 8.6GHz and 12.8GHz, respectively. Due to the higher probability of being in the center frequency band, the power spectra shape are more centralized. According to Eq. (10), for the linear dual-chirp signal, its instantaneous frequency varies from ω_{RF} to $\omega_{RF} \pm 4\beta_3 k(T/2)$ linearly within a pulse duration, and forms a bandwidth of $4\beta_3 kT$, which is four times the drive signal bandwidth B. While, for the nonlinear dual-chirp signals, their instantaneous frequencies change nonlinearly with a larger bandwidth of $2pB$ in the pulse duration, which means a larger TBWP and thus a higher pulse compression ratio. So the radar with the proposed nonlinear dual-chirp signals will have a better range resolution and velocity resolution.

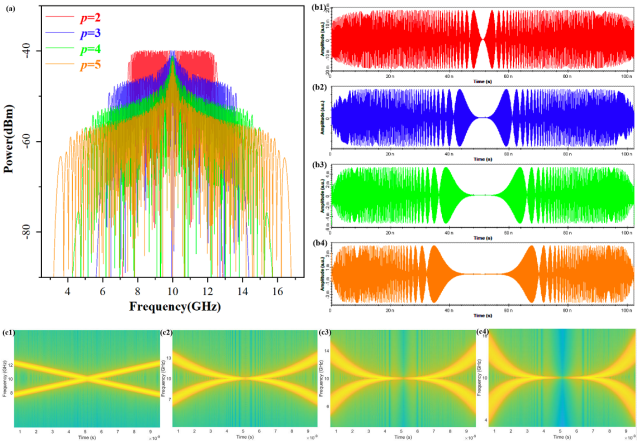

FIGURE 7. (a) dual-chirp signals spectra centered at 10GHz. When $p = 2$, 3, 4 and 5, the corresponding waveforms are (b1) (b2) (b3) and (b4); the corresponding instantaneous frequency are (c1) (c2) (c3) and (c4) respectively.

To check the pulse compression characteristics of the generated dual-chirp signals, the auto-correlation function of the linear and nonlinear dual-chirp signals are calculated and are shown in Fig. 8. It can be seen, the PSLR of the generated linear pulse is 12.8dB with a full-width at half maximum (FWHM) of 0.22ns, corresponding to a pulse compression ratio (PCR) of 465.45, which is close to the theoretical TBWP of 419.84. While the PSLR is only 13dB, which is insufficient for many particular radar applications [18]. In comparison, the nonlinear chirp signal has a PSLR up

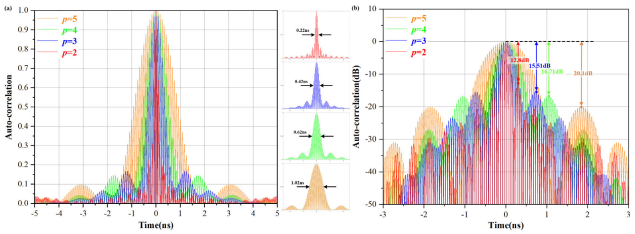

FIGURE 8. **(a) autocorrelation in linear scale, inset: zoomed-in view of the mainlobes; (b) autocorrelation in log scale.**

to 15.51dB ($p = 3$) with an FWHM of 0.42ns, 20.1dB ($p = 5$) with an FWHM of 1.02ns, as shown in Fig. 8(b). It is worth noting that the auto-correlation function of the dual nonlinear chirp signal is similar to that of the dual linear chirp signal. This difference attributes to the factor that the dual nonlinear chirp signal has an enhanced sidelobe suppression level, and as the degree of nonlinearity deepens, the PSLR will further increase. In the real applications, higher level PSLR means better multi-target resolution capability of radar and a reduced probability of false alarms. However, suppressing sidelobe is at cost of range resolution due to an increase in the width of the mainlobe. Based on the analysis of the auto-correlation function of the signals above, we can see that the generated dual-chirp signals have the good pulse compression performance.

IV. CONCLUSION

A novel photonic generation scheme of multi-band dual linear/nonlinear chirp waveform is proposed without filtering. The generated multi-frequency linear or nonlinear dual-chirp signals have a large frequency adjustable range but without undesirable chirp and high frequency components. The scheme is demonstrated by simulations, six-band dual-chirp signals generated have good pulse compression capability and can cover five radar bands, including X-band (centered at 10GHz), Ka-band (centered at 30GHz), U-band (centered at 50GHz), V-band (centered at 70GHz), and W-band (centered at 90GHz, 110GHz). Compared with the linear dual-chirp waveforms which have a bandwidth only quadrupling the drive quadratic signal, the nonlinear dual-chirp signal has larger bandwidth, $2p$ times of the drive p power function signal. According to the auto-correlation function analysis, as the power-function-type drive signal order p increases from 2(linear) to 5, the PSLR improves from 12.8dB($p = 2$) up to 20.1dB($p = 5$), which means the improvement of the radar multi-target resolution capability. Moreover, the generated nonlinear dual-chirp signal by the proposed scheme have enhanced ability of detecting multi-targets and processing signals, and is expected to be used in multi-band radar systems.

REFERENCES

[1] G. Serafino, F. Scotti, L. Lembo, B. Hussain, C. Porzi, A. Malacarne, S. Maresca, D. Onori, P. Ghelfi, and A. Bogoni, "Toward a new generation of radar systems based on microwave photonic technologies," *J. Lightw. Technol.*, vol. 37, no. 2, pp. 643–650, Jan. 15, 2019.
[2] M. Vespe, C. J. Baker, and H. D. Griffiths, "Automatic target recognition using multi-diversity radar," *IET Radar Sonar Navigat.*, vol. 1, no. 6, pp. 470–478, 2007.
[3] P. Van Dorp, R. Ebeling, and A. G. Huizing, "High resolution radar imaging using coherent multiband processing techniques," in *Proc. IEEE Radar Conf.*, Washington DC, USA, Jan. 2010, pp. 981–986.
[4] M. Richards, J. A. Scheer, and W. A. Holm, *Principle of Modern Radar: Basic Principle*. Raleigh, NC, USA: SciTech, 2010.
[5] J. Yao, "Microwave photonics," *J. Lightw. Technol.*, vol. 27, no. 3, pp. 314–335, Feb. 1, 2009.
[6] J. Capmany and D. Novak, "Microwave photonics combines two worlds," *Nature Photon.*, vol. 1, no. 6, pp. 319–330, Apr. 2007.
[7] R. Won, "Microwave photonics shines," *Nature Photon.*, vol. 5, no. 12, p. 736, 2011.
[8] X. Zou, B. Lu, W. Pan, L. Yan, A. Stöhr, and J. Yao, "Photonics for microwave measurements," *Laser Photon. Rev.*, vol. 10, no. 5, pp. 711–734, Jul. 2016.
[9] F. Zhang, Q. Guo, and S. Pan, "Photonics-based real-time ultra-high-range-resolution radar with broadband signal generation and processing," *Sci. Rep.*, vol. 7, no. 1, Dec. 2017, Art. no. 13848.
[10] Q. Guo, F. Zhang, P. Zhou, and S. Pan, "Dual-band LFM signal generation by optical frequency quadrupling and polarization multiplexing," *IEEE Photon. Technol. Lett.*, vol. 29, no. 16, pp. 1320–1323, Aug. 15, 2017.
[11] K. Zhang, S. Zhao, X. Li, Z. Zhu, W. Jiang, T. Lin, and G. Wang, "Photonic approach to dual-band dual-chirp microwave waveform generation with multiplying central frequency and bandwidth," *Opt. Commun.*, vol. 437, pp. 17–26, Apr. 2019.
[12] K. Zhang, S. Zhao, T. Lin, X. Li, W. Jiang, and G. Wang, "Photonic generation of multi-frequency dual-chirp microwave waveform with multiplying bandwidth," *Results Phys.*, vol. 13, Jun. 2019, Art. no. 102226.
[13] G. Galati, G. Pavan, and F. De Palo, "Chirp signals and noisy waveforms for solid-state surveillance radars," *Aerospace*, vol. 4, no. 1, Mar. 2017, Art. no. 4010015.
[14] J. M. Kurdzo, B. L. Cheong, R. D. Palmer, and G. Zhang, "Optimized NLFM pulse compression waveforms for high-sensitivity radar observations," in *Proc. Int. Radar Conf.*, Oct. 2014, pp. 1–6.
[15] R. Ghavamirad, H. Babashah, and M. A. Sebt, "Nonlinear FM waveform design to reduction of sidelobe level in autocorrelation function," in *Proc. Iranian Conf. Electr. Eng. (ICEE)*, May 2017, pp. 1973–1977.
[16] P. Tovar, L. E. Ynoquio Herrera, R. M. Ribeiro, and J. P. Von Der Weid, "Photonic generation of NLFM microwave pulses from DFB-laser chirp," *IEEE Photon. Technol. Lett.*, vol. 31, no. 17, pp. 1417–1420, Sep. 1, 2019.
[17] P. Zhou, R. H. Zhang, K. X. Li, Z. D. Jiang, P. H. Mu, H. L. Bao, and N. Q. Li, "Generation of NLFM microwave waveforms based on controlled period-one dynamics of semiconductor lasers," *Opt. Exp.*, vol. 28, nos. 22–26, pp. 32647–32656, 2020.
[18] M. S. Kang, B. S. Kim, H. J. Kim, and S. K. Park, "A study on pulsed-LFM and pulsed-NLFM waveforms for radar systems," in *Proc. Int. Conf. Inf. Commun. Technol. Converg. (ICTC)*, Oct. 2019, pp. 983–985.

HONGSHI ZHAO is currently pursuing the Ph.D. degree with the Beijing University of Posts and Telecommunications, Beijing, China. Her current research interests include analog optical signal processing technologies and microwave arbitrary waveform generation.

JIANXIN MA (Member, IEEE) received the Ph.D. degree in optical communication from the Beijing University of Posts and Telecommunications, Beijing, China, in 2007. He is currently a Professor with the Beijing University of Posts and Telecommunications. He has authored or coauthored more than 100 scientific publications appearing in journals or international conferences. His research interests include microwave photonics and optical communications.